


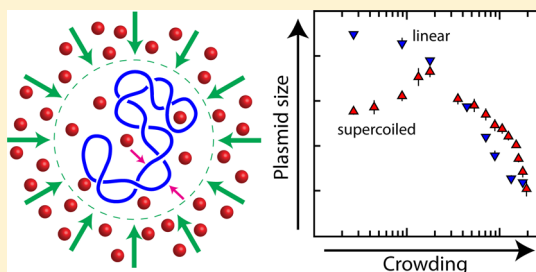
Compaction of Plasmid DNA by Macromolecular Crowding

Amar Nath Gupta and Johan R. C. van der Maarel*

Biophysics and Complex Fluids Group, Department of Physics, National University of Singapore, 2 Science Drive 3, Republic of Singapore 117542

 Supporting Information

ABSTRACT: With a view to understand compaction of DNA in crowded conditions, we have measured the radius of gyration of pHSG298 plasmid (2675 bp) in its supercoiled and linear forms and in the presence of dextran nanoparticles with light scattering. It was observed that the supercoil initially expands and subsequently compacts with increasing volume fraction of the crowder. The extent of the expansion depends on the size of the nanoparticle, with the smallest particles exhibiting the largest effect. In the case of the linear plasmid, monotonous compaction and no apex in the radius of gyration were observed. The plasmid does not collapse into a condensed state. In crowded conditions, the size of the supercoiled molecule exceeds the one of its linear variant. Supercoiling hence restrains rather than facilitates compaction of crowded DNA. Our results show two different, but closely related, aspects of the crowding phenomenon. First, the supercoil expands through a modification of its geometrical properties by the depletion induced attraction between the two opposing duplexes of the superhelix. Second, the molecule gets compressed due to the depletion of nanoparticles in the interior of the coil with concomitant imbalance in osmotic pressure between the coil and surrounding medium. The antagonistic nature of these two aspects of crowding results in a much more pronounced and richer effect on the dimensions of supercoiled plasmid than the effect of variation in ionic strength. The change in DNA dimensions as a response to crowding may have implications in biology as well as biotechnology.

 INTRODUCTION

DNA often exists in a supercoiled conformation, in which the duplex is wound around itself to form a higher order helix.¹ It is also often congested, such as in liquid crystals, the nucleoid of bacterial cells, synthetic gene transfer vectors, and porous gel materials for size exclusion chromatography.^{2–6} The conformation of the supercoil is determined by topological and geometrical properties (degree of interwinding and number of interwound branches), concentration of salts, interaction among DNA molecules at higher concentrations, and interaction with other biomolecules including neutral crowders. In order to be accommodated in a crowded state, the supercoil has to decrease its spatial extent (excluded volume) by a change in conformation. Correspondingly, DNA's conformation is modulated in response to changes in crowding through the effect on excluded volume. This plasticity of DNA shapes may have a regulatory role and be important for the postreplicative segregation of bacterial chromosomes.⁷

Supercoiled DNA can be visualized by (cryo)electron and atomic force microscopy.^{8,9} It has been observed that the distance between the two opposing duplexes in the superhelix (interduplex distance) is inversely proportional to the superhelical density and decreases with increased concentration of salt. These imaging techniques are however not well adapted to the investigation of three-dimensional solution properties such as excluded volume. Size-related properties are best and quantitatively inferred from scattering experiments using liquid samples representative of the native state. The interwound

conformation of supercoiled plasmid (2.7 kbp) has previously been investigated with small-angle neutron scattering.^{10–12} It was found that the interduplex distance decreases with increased salt and/or DNA concentration (DNA–DNA crowding). The overall size of the supercoil, that is, its radius of gyration R_g , can be determined by static light scattering. With this method it was found that supercoiled plasmid has a 30–45% smaller size than its linear isoform, but no significant change in R_g with concentration of salt was observed.^{13–15} Note that these results were obtained for DNAs dispersed in solutions of salts without crowding agents.

Here, we investigate the compaction of a supercoiled plasmid (pHSG298, 2675 bp) by the generic crowding agent dextran. In the present buffer conditions, the molecules do not collapse into a condensed state. Dextran is a neutral branched polysaccharide made of glucose monomers. The dextran molecules used in this study have a radius of gyration d in the range 2.6–17 nm. They are spherical nanoparticles and readily dissolve in water. Dextran is often used to mimic the intracellular crowded environment *in vitro*.¹⁶ We isolated and purified plasmid in the supercoiled and linear isoforms. These isoforms were dispersed in an aqueous buffer with various amounts of dextran, and their sizes (R_g) were measured with Rayleigh light scattering. Sufficiently diluted samples were used

Received: December 20, 2016

Revised: January 30, 2017

Published: February 16, 2017

to ensure minimal inter-DNA interference and minimal effect of DNA–DNA crowding on the conformation of the plasmids. For reference, R_g of the plasmids in crowder-free solution, but in the presence of various concentrations of salt, was also measured. The results are discussed in terms of the geometric properties of the supercoil as well as osmotic effects induced by the depletion interaction between DNA and the crowding nanoparticles.

EXPERIMENTAL PROCEDURES

Preparation of the Cell Paste. BL21 bacteria transformed with pHSG298 were grown on a Luria Broth (LB) plate with kanamycin (25 mg/L). A single colony was taken to grow a starter culture in LB medium containing kanamycin at 310 K for 8 h (OD600 = 0.8). The starter culture was diluted 1000 times into LB medium containing kanamycin and grown at 310 K for 12–16 h with vigorous shaking (280 rpm, OD600 = 1.8 for each batch). The cells were harvested by centrifugation at 6000g for 15 min at 277 K.

Plasmid Extraction and Purification. The bacterial pellet was suspended in 0.5 L of 50 mM Tris-HCl buffer, pH 7.5, 10 mM EDTA, and subsequently lysed with 0.5 L of an alkaline solution (0.2 M NaOH, 1% SDS) at room temperature. The pH of the cell suspension and the alkaline solution was maintained below 12.5. Genomic DNA, cell debris, and proteins were precipitated by the addition of 0.5 L of 3 M potassium acetate, pH 5.5, prechilled at 277 K. After centrifugation at 20000g for 30 min at 277 K, the supernatant was pumped through a Sepharose 6 fast flow column (XK 50/30) equilibrated with 2 M $(\text{NH}_4)_2\text{SO}_4$, 10 mM EDTA, and 100 mM Tris-HCl, pH 7.0, with an AKTA explorer chromatography system (GE Life Sciences, columns and chromatography media were also purchased from GE). This gel filtration step results in the removal of RNA. The plasmid was further purified by thiophilic interaction chromatography using a column with PlasmidSelect, equilibrated with the above-mentioned 2 M $(\text{NH}_4)_2\text{SO}_4$ buffer, and eluted with a gradient to 0.4 M NaCl, 2 M $(\text{NH}_4)_2\text{SO}_4$, 10 mM EDTA, and 100 mM Tris-HCl, pH 7.0.¹⁷ Finally, the sample was concentrated and endotoxins were removed by capturing the plasmid on a Source 30Q ion exchange column followed by elution in a gradient to 0.6 M NaCl. After precipitation with isopropanol, the DNA was gently dried for a short period, dissolved in 1×TE (10 mM Tris, 1 mM EDTA, pH 8) buffer, and stored at 277 K. We have obtained a reasonably good quality of the supercoiled plasmid by optimization of the purification protocol through a longer concentration gradient in the elution of the Sepharose column. As byproduct, we obtained the purified pHSG298 plasmid in the linearized form.

Plasmid Characterization. UV spectroscopy showed that the ratio of the optical absorbance at 260 and 280 nm (A_{260}/A_{280}) exceeded 1.8, indicating that the preparation was free of protein. The integrity of the plasmid was checked with 0.8% agarose electrophoresis gel in TAE buffer (40 mM Tris-acetate, 1 mM EDTA, pH 8.3) at 70 V for 2 h.¹⁸ The gel image is shown in Figure S1. The linking number deficit and percentage of open circular plasmid were determined by a series of 1.4% agarose electrophoresis gels in TPE buffer (90 mM Tris-phosphate, 1 mM EDTA, pH 8.3) at 50 V for 36 h with chloroquine phosphate concentrations of 1, 3, 5, 10, 20, 40, 80, and 120 mg/L.^{1,19} The positions of the bands pertaining to $\Delta Lk = 0$ and ± 1 were determined by (partial) relaxation of the plasmid with topoisomerase II (Affymetrix). We observed optimal separation of the topoisomers at chloroquine phosphate concentrations of 3 and 80 mg/L. At these concentrations all topoisomers are either negatively (3 mg/L) or positively (80 mg/L) supercoiled. The gel images obtained with chloroquine phosphate concentrations of 1, 3, and 80 mg/L are shown in Figure S2. In the series of gels with increasing concentration of the intercalator, we counted a linking number deficit $\Delta Lk = -9 \pm 2$ (superhelical density $\sigma = -0.035$) pertaining to the most abundant topoisomer. About 5% of the plasmid is nicked and open circular.

Sample Preparation. All samples were prepared with a final DNA concentrations c_{DNA} of 50 mg/L. Dextran with molecular weights of 5, 50, and 410 kg/mol was purchased from Sigma-Aldrich. The buffer solvents are 0.4×TE with added NaCl and 1×TE with added dextran.

Solutions of supercoiled and linearized plasmid and the relevant solvent were mixed and incubated for at least 24 h at 277 K. Prior to light scattering measurements, solvent and samples were filtered through 0.02 and 0.22 μm Whatman syringe filters, respectively. The final DNA concentration (after filtration) was determined by UV–vis spectroscopy.

Light Scattering. Light scattering measurements were done with a Wyatt DAWN 8+ multiangle light scattering instrument (Goleta, CA). The incident light source was a GaAs diode laser (50 mW) generating vertically polarized light of 658 nm wavelength. Scattered light is simultaneously measured by eight photodetectors at angles spaced between 15° and 160° with respect to the incident beam. This allows a momentum transfer range of $(0.3\text{--}2.5) \times 10^7 \text{ nm}^{-1}$. The plasmid samples were slowly injected into the flow cell of the light scattering instrument to avoid any structural changes due to pressure. A baseline was determined by measuring the scattering from the buffer at the beginning as well as at the end of the sample injection. Data reduction with Wyatt's ASTRA software allowed subtraction of the baseline solvent scattering and the determination of the excess Rayleigh ratio R_θ .

RESULTS

For pHSG298 plasmid, with dimensions of less than 100 nm, the overlap concentration between the dilute and the semidilute regime is around 3 g/L. The latter concentration exceeds the concentration employed in the light scattering experiments (50 mg of DNA/L) by 2 orders of magnitude. At such a low concentration interference among different DNA molecules is negligible (to be confirmed below). Furthermore, we have checked that the scattered intensity recorded at an angle of 90° from a plasmid solution and a typical mixture of plasmid and dextran exceeds the intensity pertaining to the corresponding dextran solution by a factor of 30 and 40, respectively. Accordingly, the scattering is dominated by DNA and the contribution from dextran is negligible. The excess Rayleigh ratio is then proportional to the DNA form factor $P(q)$ according to $R_\theta = K^*cM_wP(q)$, with K^* an optical constant, c the concentration of DNA, and M_w the DNA molar mass. Momentum transfer q is defined by the wavelength λ , refractive index of the solvent n_0 , and scattering angle θ according to $q = 4\pi n_0/\lambda \sin(\theta/2)$. The optical constant $K^* = 4\pi^2 n_0^2 (dn/dc)^2 / (\lambda^4 N_A)$, with Avogadro's number N_A , was calculated with the differential refractive index increment $dn/dc = 0.17 \text{ L/kg}$ for DNA.²⁰ Some examples of partial Zimm plots, that is K^*c/R_θ versus q^2 , are shown in panels A and B of Figure 1 for linear and

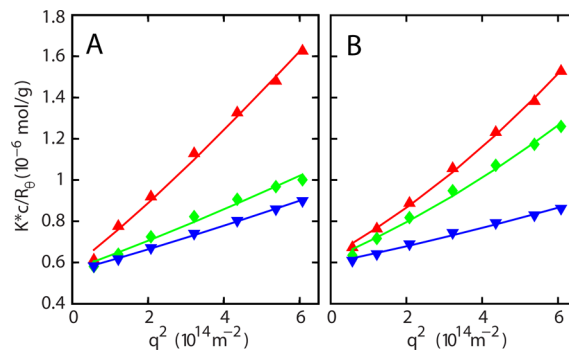


Figure 1. (A) Partial Zimm plot for linear plasmid in 1×TE with 2 (red \blacktriangle), 10 (green \blacklozenge), and 20 (blue \blacktriangledown) g of dextran/L. Dextran size $d = 2.6 \text{ nm}$. (B) As in panel A, but for supercoiled plasmid in 1×TE with 1 (red \blacktriangle), 4 (green \blacklozenge), and 12 (blue \blacktriangledown) g of dextran/L and dextran size $d = 6.9 \text{ nm}$. The curves represent fits of the relevant form factors.

supercoiled plasmid in 1×TE (10 mM Tris, 1 mM EDTA, pH 8) buffer, respectively. Note that $P(q)$ is normalized to unity for $q \rightarrow 0$, so that M_w^{-1} can be obtained from the y -axis intercept. The radius of gyration R_g is obtained from a fit of the relevant form factor $P(q)$ to K^*c/R_θ at higher values of momentum transfer.

For the linear isoform, the data are analyzed with an approximate $P(q)$ pertaining to a linear, semiflexible polymer with excluded volume effects.²¹ To the best of our knowledge, a general expression for $P(q)$ of supercoiled DNA is not available. Our previously reported expression is only valid for high values of q exceeding the inverse interdplex distance.¹¹ The present light scattering experiments are performed in the low q range with $0.25 \lesssim qR_g \lesssim 2$. Furthermore, our closed circular plasmid is moderately supercoiled (superhelical density $\sigma \sim -0.035$) and can to a good approximation be considered a semiflexible ring. Accordingly, we have used the low qR_g approximation of $P(q)$ pertaining to a ring polymer with excluded volume interaction.²² The utilized expressions for $P(q)$ are summarized in the Supporting Information. Examples of the fits are shown in Figure 1. In particular deviations from linearity at larger values of q^2 are well described. For dextran-crowded plasmid, the fitted values of M_w are shown in Figure 2. The values of R_g

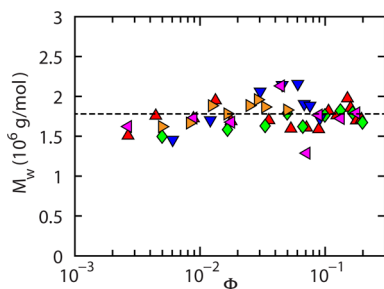


Figure 2. Molecular mass M_w of linear (magenta ◀, gold ▶) and supercoiled (red ▲, green ◆, blue ▼) plasmid in 1×TE versus dextran volume fraction Φ . Dextran size $d = 2.6$ (red ▲, magenta ◀), 6.9 (green ◆, gold ▶), and 17 (blue ▼) nm. The dashed line denotes the calculated value for pHSG298, that is, 1.78×10^6 g/mol.

of supercoiled plasmid crowded by dextran of various size are displayed in Figure 3A. For the sake of comparison, R_g pertaining to linear and supercoiled plasmid dispersed in buffers of various ionic strength but without dextran is shown in

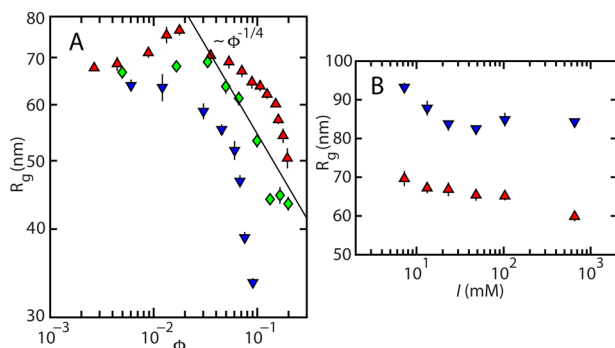


Figure 3. (A) Radius of gyration R_g of supercoiled plasmid in 1 × TE versus volume fraction Φ of dextran with size $d = 2.6$ (red ▲), 6.9 (green ◆), and 17 (blue ▼) nm. The solid line represents $\Phi^{-1/4}$ scaling. (B) Radius of gyration R_g of linear (blue ▼) and supercoiled (red ▲) plasmid versus ionic strength I .

Figure 3B. The effect of the topological constraint (supercoiled versus linear) on R_g of dextran-crowded plasmid is displayed in Figure 4. We have verified that inclusion of self-avoidance in the data analysis results in no appreciable differences in M_w and marginal differences in R_g of less than 3%.

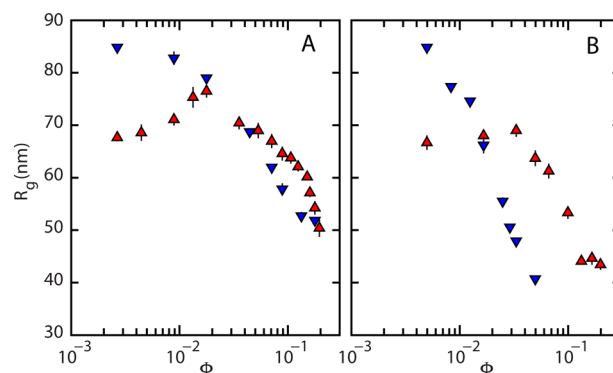


Figure 4. (A) Radius of gyration R_g of linear (blue ▼) and supercoiled (red ▲) plasmid in 1×TE versus volume fraction Φ of dextran with size $d = 2.6$ nm. (B) As in panel A, but for dextran with size $d = 6.9$ nm.

Based on the base pair sequence, the calculated $M_w = 1.78 \times 10^6$ g/mol. For the dextran-crowded samples, the averaged experimental value $M_w = (1.8 \pm 0.2) \times 10^6$ g/mol. No systematic variation is observed, irrespective DNA topology, dextran size, and volume fraction (see Figure 2). The agreement between the experimental and calculated molecular weights confirms the negligible contribution to the scattering from dextran, insignificant plasmid aggregation or catenation, and insignificant interference among different DNA molecules.

For supercoiled, crowder-free plasmid in 1×TE buffer (ionic strength of 10.7 mM), R_g takes a value of 67 ± 1 nm. This value is in fair agreement with the literature R_g values of 102 ± 2 , 82 ± 3 , and 56 ± 4 nm for 5.8, 3.7, and 2.7 kbp supercoiled DNA, respectively.^{13–15} Furthermore, the smaller size of supercoiled plasmid with respect to its linear isoform (in crowder-free conditions) and the moderate decrease in size with increasing ionic strength agree with previously reported results.^{14,15}

The presence of the dextran nanoparticles impacts the size of both supercoiled and linear DNA. In the limit of vanishing volume fraction of dextran, the measured values of R_g in 1×TE buffer approach the values obtained in 0.4×TE buffer with added NaCl at the relevant ionic strength of 10.7 mM. For supercoiled plasmid and smaller dextran size ($d \lesssim 6.9$ nm), R_g first increases, exhibits an apex, and subsequently decreases with increasing volume fraction of dextran. For the larger dextran particles of size $d = 17$ nm, R_g decreases monotonously and no apex is observed (see Figure 3A). In the case of the linear plasmid and irrespective dextran size, R_g decreases monotonously with increasing volume fraction of dextran (Figure 4). In the present experimental conditions, the plasmid gets compacted but does not collapse into a condensed state (no condensation). For polymer induced condensation, it is necessary to increase the concentration of monovalent salts to hundreds of millimolar and/or to confine the DNA molecule in a nanopore.^{23,24} Since these conditions are not met in our experimental approach, we do not observe a plateau in R_g at high volume fractions of crowder (up to $\phi = 0.2$). For both supercoiled and linear plasmid, the compaction is highly depended on nanoparticle size, with the largest particles being

the most effective. Under minimal or no crowding conditions, the size of supercoiled plasmid is smaller than the size of its linear variant. Accordingly, supercoiling has been identified as a compaction mode, in the sense that it reduces the spatial extent of the molecule.¹ A new result is that in crowded conditions the situation may be reversed. At higher volume fractions of crowder, supercoiled plasmid takes a more extended conformation (larger R_g values) than the linear one. Hence, to a certain extent, supercoiling restrains compaction of DNA by macromolecular crowding. Finally, it should be noted that irrespective of topological constraint, the reduction in plasmid size by crowding far exceeds the one caused by an increase in ionic strength (Figure 3).

DISCUSSION

Neutral dextran particles with a size of several nanometers penetrate the DNA coil, but they are not known to bind and/or change the mechanical properties of the duplex. However, each segment of the DNA molecule is surrounded by a cylindrical volume in which the nanoparticles cannot penetrate for steric reasons. The effect of this volume interaction is twofold: (i) the geometrical properties of the supercoil change through an attractive force between almost (anti)parallel DNA segments and (ii) the coil gets compressed through an imbalance in osmotic pressure between the interior of the coil and the surrounding medium. The former effect is of particular importance for a superhelix, in which a duplex is wound around another duplex of the same molecule in an antiparallel configuration. Osmotic compression is important irrespective of DNA topology. Accordingly, in order to understand compaction, these two aspects of the crowding phenomenon need to be evaluated and gauged against our observations.

An important feature of supercoiling is that it provides a mechanism to bring distant DNA sections, which are separated over a large distance along the contour, close together spatially.^{1,26} A schematic drawing of a nonbranched supercoil is shown in Figure 5A. Note that a supercoil of the present molecular weight may be branched, but this is irrelevant for the present discussion. The two opposing duplexes are antiparallel and separated by a distance r in the direction perpendicular to the central axis of the supercoil. Each duplex is surrounded by a cylindrical depletion zone of diameter $D + d$, with D and d being the diameter of the duplex and nanoparticle, respectively. As illustrated in Figure 5B, for interduple distance r in the range $D < r < D + d$ there is an attractive force due to the overlap of the depletion zones with concomitant increase in accessible volume to the nanoparticles.²⁷ In crowded conditions, the supercoil is effectively confined within a cylindrical volume with a diameter equal to the sum of the diameter of the duplex and size of the crowder, that is, $D + d$. Note that a reduction in interduple distance by increasing concentration of plasmid (DNA–DNA crowding) has previously been inferred from neutron scattering and Monte Carlo simulation.¹²

The interwound supercoil can be considered a wormlike chain set out by the central (plectonemic) axis with length L_{plec} and bending persistence length P_{plec} . The persistence length is the projection of the persistence lengths of the two opposing duplexes (each with persistence length P) onto the central axis, that is, $P_{\text{plec}} = 2P \cos \theta$ with θ the angle enclosed by the duplex's tangent vector and the central axis. The length of the central axis L_{plec} , angle θ , and persistence length P_{plec} can be obtained by minimization of the molecular free energy of the supercoil

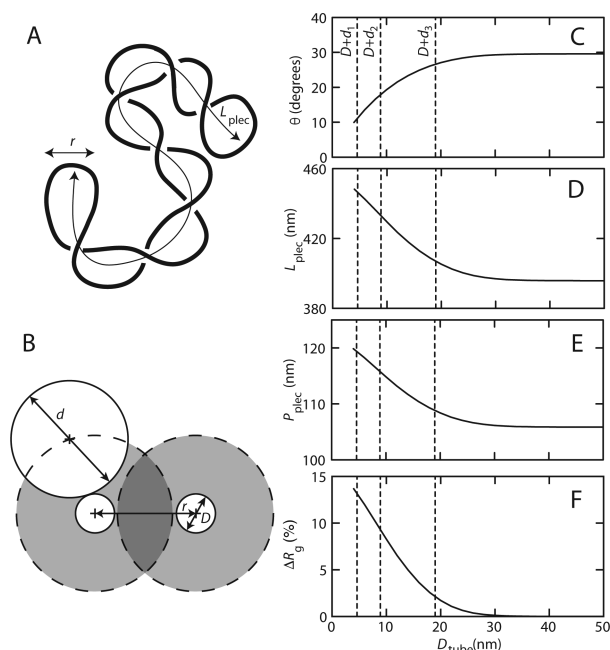


Figure 5. (A) Schematic drawing of a supercoil with interduple distance r and length of the superhelical axis L_{plec} . (B) Cross section of two opposing duplexes, each of diameter D , each surrounded by a depletion zone $d/2$, and separated by distance r . Note that the depletion zones overlap for $D < r < D + d$. (C) Angle θ enclosed by the duplex's tangent vector and the superhelical axis versus the diameter of the confining volume D_{tube} resulting from molecular free energy minimization.²⁵ The dashed lines demarcate the range of the attractive depletion interaction for dextran sizes $d_1 = 2.6$, $d_2 = 6.9$, and $d_3 = 17$ nm (duplex diameter $D = 2$ nm). (D) As in panel C, but for L_{plec} . (E) As in panel C, but for the persistence length of the superhelical axis P_{plec} . (F) As in panel C, but for the relative change in R_g .

including elastic, electrostatic, and entropic contributions.^{26,28,29} With a similar theoretical approach, we obtained these structural parameters for a supercoil subjected to confinement within a cylindrical volume with diameter D_{tube} .²⁵ Results are shown in panels C–E of Figure 5. With increasing confinement (smaller values of D_{tube}), both L_{plec} and P_{plec} are seen to increase due to increasing alignment (smaller values of θ) of the segments. The supercoil expands due to this increase in length and bending rigidity of the superhelical axis.

With the contour and persistence length of the superhelical axis, R_g of a nonbranched, wormlike supercoil can be calculated with the Benoit–Doty equation.^{26,30} Note that there are only a few Kuhn segments per supercoil [$L_{\text{plec}}/(2P_{\text{plec}}) \sim 2$], so that swelling due to self-avoidance is negligible. However, the absolute value of the calculated R_g bears little relevance because the real supercoil is smaller in size than the hypothetical linear one due to branching. Accordingly, in Figure 5F the relative change in R_g with respect to the unconfined situation is depicted. In crowded conditions, the supercoil is effectively confined within a tube with diameter $D_{\text{tube}} \simeq D + d$. For confinement within a range corresponding to the size of the smallest nanoparticles, the predicted increase in R_g is $\sim 14\%$. For the particles of intermediate size, the increase is $\sim 10\%$, whereas for the largest particles the effect is minimal with an increase of $\sim 2\%$. These theoretical predictions for the increase in R_g are in almost quantitative agreement with the experimentally observed apex in R_g for the plasmid in the

supercoiled form (see Figure 3A). A change in geometrical properties associated with supercoiling is obviously irrelevant for the linear isoform, and hence, no apex in R_g is observed (Figure 4).

In the interior of the coil, the nanoparticle density is depleted due to the hard-core repulsion between the nanoparticles and DNA. The concomitant difference in osmotic pressure between the coil and surrounding medium results in compression of the coil, irrespective of supercoiling. We will now derive a scaling theory describing the effect of size and density of the crowder on plasmid dimensions. For simplicity, we assume that the statistics is ideal. This assumption is supported by the notion that the number of Kuhn segments is small, so that self-avoidance is negligible. The free energy of compression is then inversely proportional to R_g^2 , that is, $F_{\text{elas}}/kT \simeq (R_g^0/R_g)^2$ with R_g^0 the radius of gyration in the absence of the compressing force.³¹ The elastic pressure follows from the derivative of the elastic free energy to the volume of the coil ($V \simeq R_g^3$) and reads $\Pi_{\text{elas}} \simeq kTR_g^0^2/R_g^5$. A scaling relation for the work of inserting a nanoparticle into the coil can be derived following a procedure originally due to de Gennes.³² The work is on the order of thermal energy and proportional to the ratio of the particle and coil size, that is, $w/kT \simeq d/R_g$ (again, we assume ideal statistics). The coil is immersed in a medium with nanoparticle density ρ . From the balance in chemical potentials, the difference in particle density between the interior and surrounding medium is to leading order given by $\Delta\rho \simeq \rho d/R_g$ ($d \ll R_g$). With a typical experimental ratio $d/R_g \simeq 0.05$, the particle density is depleted by a few percent. The osmotic pressure $\Pi_{\text{osmo}} \simeq kT\Delta\rho$ should balance the elastic pressure $\Pi_{\text{osmo}} = \Pi_{\text{elas}}$ from which follows the scaling relation $R_g \simeq R_g^0^{1/2} \rho^{-1/4} d^{-1/4}$. In terms of the volume fraction of the nanoparticles ($\phi \simeq \rho d^3$), this expression takes the form $R_g \simeq R_g^0^{1/2} d^{1/2} \phi^{-1/4}$. At the onset of compaction $R_g \simeq R_g^0$, which sets a critical volume fraction $\phi^* \simeq (d/R_g^0)^2$. Accordingly, for linear DNAs the radius of gyration is already seen to decrease for volume fractions below 0.01. The decrease in R_g with increasing volume fraction is reasonably well described by the predicted $\Phi^{-1/4}$ scaling (this is particularly the case for the particles of intermediate size; see Figure 3A). However, the scaling theory does not correctly predict the strong dependence of R_g on the size of the nanoparticles. This might be related to the above-described modification of the geometrical properties of the supercoil, which calls for a more detailed expression for the work of insertion. In view of the many uncertain parameters describing the intricate interaction between nanoparticles and supercoiled DNA, we refrain from further elaboration.

CONCLUSIONS

With a view to understand compaction of DNA by crowding, we have measured the radius of gyration of a plasmid in its supercoiled and linear form and in the presence of neutral nanoparticles. The plasmid is sufficiently diluted, so that there is no significant DNA–DNA interaction. Our results show that in the context of supercoiling the crowding phenomenon has two aspects. First, the interdplex distance decreases, with a concomitant increase in length and bending rigidity of the superhelical axis. This is due to the depletion of nanoparticles in the overlap region between the two opposing duplexes of the superhelix. Through this change in geometrical properties, the supercoil expands. The interdplex distance becomes around the range of the attractive force, that is, the sum of the diameters of the duplex and nanoparticle. The decrease in

interduplex distance with concomitant expansion of the supercoil is hence more conspicuous for crowders of smaller size. For larger nanoparticles, the range of attraction may exceed the diameter of the supercoil in the crowder-free state. In this situation, there is no effective confinement and hence no crowder-induced expansion of the supercoil. A second aspect of crowding is that the nanoparticle density in the interior of the coil is depleted, which results in an imbalance in osmotic pressure between the coil and the surrounding medium. The plasmid gets compacted, irrespective of topology, but does not collapse into a condensed state. The antagonistic nature of these two aspects of crowding has the effect that the size of supercoiled plasmid first increases, reaches an apex, and subsequently decreases with increased crowding. The maximum depends on the extent of the crowder-induced expansion, with the highest apex for the smallest crowders and vanishingly small or no apex for crowders of size equal to or larger than the interdplex distance in the crowder-free state. In the case of a linear plasmid, the only relevant mechanism is osmotic compression. Accordingly, the size of the linear plasmid decreases monotonously, and no apex is observed. A striking result is that in crowded conditions the size of supercoiled plasmid may exceed the one of its linear variant. In this situation, supercoiling restrains rather than facilitates compaction of DNA. Overall, macromolecular crowding in combination with supercoiling has a much more pronounced and richer effect on plasmid size than the effect of variation in ionic strength. This may have implications for the tuning of favorable configurational states of the genetic material in biology as well as biotechnology.

ASSOCIATED CONTENT

Supporting Information

The Supporting Information is available free of charge on the ACS Publications website at DOI: 10.1021/acs.macromol.6b02742.

Form factor expressions for linear and circular semiflexible polymers, agarose gel electrophoresis of closed circular and linear plasmid, and gel electrophoresis with chloroquine staining for linking number determination (PDF)

AUTHOR INFORMATION

Corresponding Author

*E-mail: johanmaarel@gmail.com.

ORCID

Johan R. C. van der Maarel: 0000-0001-5560-0298

Present Address

A.N.G.: Biophysics Laboratory, Department of Physics, IIT Kharagpur, India 721302.

Notes

The authors declare no competing financial interest.

ACKNOWLEDGMENTS

We thank Renko de Vries and Veronique Arluison for discussion. This research was supported by grant MOE2014-T2-1-001 of Singapore's Ministry of Education.

REFERENCES

(1) Bates, A. D.; Maxwell, A. *DNA Topology*; Oxford University Press: New York, 2005.

- (2) Reich, Z.; Wachtel, E. J.; Minsky, A. Liquid-crystalline mesophases of plasmid DNA in bacteria. *Science* **1994**, *264*, 1460–1463.
- (3) Zakharova, S. S.; Jesse, W.; Backendorf, C.; van der Maarel, J. R. C. Liquid crystal formation in supercoiled DNA solutions. *Biophys. J.* **2002**, *83*, 1119–1129.
- (4) Cunha, S.; Woldringh, C. L.; Odijk, T. Polymer-mediated compaction and internal dynamics of isolated *Escherichia coli* nucleoids. *J. Struct. Biol.* **2001**, *136*, 53–66.
- (5) Korobko, A. V.; Backendorf, C.; van der Maarel, J. R. C. Plasmid DNA encapsulation within cationic diblock copolymer vesicles for gene delivery. *J. Phys. Chem. B* **2006**, *110*, 14550–14556.
- (6) Stadler, J.; Lemmens, R.; Nyhammar, T. Plasmid DNA purification. *J. Gene Med.* **2004**, *6* (S1), S54–S66.
- (7) Benedetti, F.; Japaridze, A.; Dorier, J.; Racko, D.; Kwapich, R.; Burnier, Y.; Dietler, G.; Stasiak, A. Effects of physiological self-crowding of DNA on shape and biological properties of DNA molecules with various levels of supercoiling. *Nucleic Acids Res.* **2015**, *43*, 2390–2399.
- (8) Boles, T. C.; White, J. H.; Cozzarelli, N. R. Structure of plectonemically supercoiled DNA. *J. Mol. Biol.* **1990**, *213*, 931–951.
- (9) Lyubchenko, Y.; Shlyakhtenko, L. Visualization of supercoiled DNA with atomic force microscopy in situ. *Proc. Natl. Acad. Sci. U. S. A.* **1997**, *94*, 496–501.
- (10) Hammermann, M.; Brun, N.; Klenin, K. V.; May, R.; Tóth, K.; Langowski, J. Salt-dependent DNA superhelix diameter studied by small angle neutron scattering measurements and Monte Carlo simulations. *Biophys. J.* **1998**, *75*, 3057–3063.
- (11) Zakharova, S. S.; Jesse, W.; Backendorf, C.; Egelhaaf, S. U.; Lapp, A.; van der Maarel, J. R. C. Dimensions of plectonemically supercoiled DNA. *Biophys. J.* **2002**, *83*, 1106–1118.
- (12) Zhu, X.; Ng, S. Y.; Gupta, A. N.; Feng, Y. P.; Ho, B.; Lapp, A.; Egelhaaf, S. U.; Forsyth, V. T.; Haertlein, M.; Moulin, M.; Schweins, R.; van der Maarel, J. R. C. Effect of crowding on the conformation of interwound DNA strands from neutron scattering measurements and Monte Carlo simulations. *Phys. Rev. E* **2010**, *81*, 061905.
- (13) Fishman, D. M.; Patterson, G. D. Light scattering studies of supercoiled and nicked DNA. *Biopolymers* **1996**, *38*, 535–552.
- (14) Langowski, J.; Hammermann, M.; Klenin, K.; May, R.; Tóth, K. Superhelical DNA studied by solution scattering and computer models. *Genetica* **1999**, *106*, 49–55.
- (15) Latulippe, D. R.; Zydney, A. L. Radius of gyration of plasmid DNA isoforms from static light scattering. *Biotechnol. Bioeng.* **2010**, *107*, 134–142.
- (16) Zimmerman, S. B.; Minton, A. P. Macromolecular crowding: biochemical, biophysical, and physiological consequences. *Annu. Rev. Biophys. Biomol. Struct.* **1993**, *22*, 27–65.
- (17) Sandberg, L. M.; Bjurling, Å.; Busson, P.; Vasi, J.; Lemmens, R. Thiophilic interaction chromatography for supercoiled plasmid DNA purification. *J. Biotechnol.* **2004**, *109*, 193–199.
- (18) Backendorf, C.; Olsthoorn, R.; van de Putte, P. Superhelical stress restrained in plasmid DNA during repair synthesis initiated by the UvrA, B and C proteins in vitro. *Nucleic Acids Res.* **1989**, *17*, 10337–10351.
- (19) Shure, M.; Pulleyblank, D. E.; Vinograd, J. The problems of eukaryotic and prokaryotic DNA packaging and in vivo conformation posed by superhelix density heterogeneity. *Nucleic Acids Res.* **1977**, *4*, 1183–1206.
- (20) Liang, D.; Luu, Y. K.; Kim, K.; Hsiao, B. S.; Hadjiargyrou, M.; Chu, B. In vitro non-viral gene delivery with nanofibrous scaffolds. *Nucleic Acids Res.* **2005**, *33*, e170.
- (21) Pedersen, J. S.; Schurtenberger, P. Scattering functions of semiflexible polymers with and without excluded volume effects. *Macromolecules* **1996**, *29*, 7602–7612.
- (22) Calabrese, P.; Pelissetto, A.; Vicari, E. Structure factor of dilute ring polymers. *J. Chem. Phys.* **2002**, *116*, 8191–8197.
- (23) Bloomfield, V. A. DNA condensation. *Curr. Opin. Struct. Biol.* **1996**, *6*, 334–341.
- (24) Zhang, C.; Shao, P. G.; van Kan, J. A.; van der Maarel, J. R. C. Macromolecular crowding induced elongation and compaction of single DNA molecules confined in a nanochannel. *Proc. Natl. Acad. Sci. U. S. A.* **2009**, *106*, 16651–16656.
- (25) Lim, W.; Ng, S. Y.; Lee, C.; Feng, Y. P.; van der Maarel, J. R. C. Conformational response of supercoiled DNA to confinement in a nanochannel. *J. Chem. Phys.* **2008**, *129*, 16S102.
- (26) van der Maarel, J. R. C. *Introduction to Biopolymer Physics*; World Scientific: 2008.
- (27) Asakura, S.; Oosawa, F. Interaction between particles suspended in solutions of macromolecules. *J. Polym. Sci.* **1958**, *33*, 183–192.
- (28) Marko, J.; Siggia, E. Statistical mechanics of supercoiled DNA. *Phys. Rev. E: Stat. Phys., Plasmas, Fluids, Relat. Interdiscip. Top.* **1995**, *52*, 2912–2938.
- (29) Ubbink, J.; Odijk, T. Electrostatic-undulatory theory of plectonemically supercoiled DNA. *Biophys. J.* **1999**, *76*, 2502–2519.
- (30) Benoit, H.; Doty, P. Light scattering from non-Gaussian chains. *J. Phys. Chem.* **1953**, *57*, 958–963.
- (31) Grosberg, A. Y.; Khokhlov, A. R. *Statistical Physics of Macromolecules*; AIP: Woodbury, NY, 1994.
- (32) de Gennes, P. G. Suspensions colloïdales dans une solution de polymeres. *C. R. Acad. Sci.* **1979**, *288*, 359–361.